Colorless grating couplers realized by interleaving dispersion engineered subwavelength structures

Xiaochuan Xu,[1,*] Harish Subbaraman,[2] John Covey,[1] David Kwong,[1] Amir Hosseini,[2] and Ray T. Chen[1,3]

[1]*Department of Electrical and Computer Engineering, The University of Texas at Austin, 10100 Burnet Road, Bldg. 160, Austin, Texas 78758, USA*

[2]*Omega Optics, Inc., 10306 Sausalito Drive, Austin, Texas 78759, USA*

[3]*e-mail: raychen@uts.cc.utexas.edu*

**Corresponding author: xiaochuan.xu@utexas.edu*

Received August 6, 2013; accepted August 12, 2013;
posted August 20, 2013 (Doc. ID 195320); published September 9, 2013

We investigate the waveguide dispersion of subwavelength structures, and propose that the waveguide dispersion can be reduced by reducing the period of subwavelength structures. A 3 dB bandwidth increment of 20% has been observed by introducing this concept into previously demonstrated grating couplers. To fully exploit the bandwidth merits of the structures, gratings with interleaved subwavelength structures were designed and fabricated. Two typical types of interleaving geometries have been investigated. Both demonstrated a 1 dB bandwidth ~70 nm, a 3 dB bandwidth ~117 nm, and a peak efficiency ~ − 5.1 dB at 1570 nm for transverse-electric polarized light. The simulation confirms that the dispersion engineering adds an extra 12 nm to the 1 dB bandwidth.

OCIS codes: (050.6624) Subwavelength structures; (050.2770) Gratings; (130.3120) Integrated optics devices.
http://dx.doi.org/10.1364/OL.38.003588

The past decade has witnessed a rapid development of silicon photonics [1,2]. One of the intrinsic obstacles that remains is the low fiber-to-chip coupling efficiency. This issue stems from the high index contrast between silicon and its cladding materials (air, silicon dioxide, etc.). High index contrast enables compact photonic devices, but the traditional method of coupling light into and out of these devices through fiber butt coupling is inefficient. This technique suffers from high losses induced by both the large mode area mismatch and the large effective index mismatch between the conventional single mode fiber (SMF) and the silicon strip waveguides with submicron cross sections. One of the promising solutions for achieving efficient coupling is through using grating couplers [3–11]. Grating couplers have demonstrated impressive performance features, especially the feasibility of achieving inline testing capability, which distinguishes it from edge coupling solutions. However, compared to the wideband operation of over several hundred nanometers offered by other competitive coupling solutions, such as inverse tapers [4,12–15], grating couplers suffer from poor bandwidth of tens of nanometers. Generally, the 1 dB bandwidth of a grating coupler can be estimated by the following equation [5]:

$$\Delta\lambda_{1\ \mathrm{dB}} = \eta_{1\ \mathrm{dB}} \left| \frac{-n_c \cos\theta}{\frac{1}{\Lambda_G} - \frac{dn_{\mathrm{eff}}(\lambda)}{d\lambda}} \right|. \quad (1)$$

Here, Λ_G is the period of the grating. n_c is the refractive index of the top cladding, θ is the coupling angle, and $\eta_{1\ \mathrm{dB}}$ is a fiber related constant. The waveguide dispersion term in the denominator, $(dn_{\mathrm{eff}}(\lambda)/d\lambda)$, generally has a negative sign. The above equation indicates that the bandwidth of a grating coupler can be improved through increasing the grating period Λ_G and/or reducing the waveguide dispersion $(dn_{\mathrm{eff}}(\lambda)/d\lambda)$. The waveguide dispersion can be reduced by abating the effective index or tuning the aspect ratio of a waveguide. Reducing the average effective index of the grating is the most effective way of altering the dispersion relation because light becomes loosely confined as the effective index decreases [5], thereby rendering the waveguide boundary less sensitive to wavelength. For conventional silicon waveguides, the waveguide dispersion cannot be controlled effectively because the refractive index of silicon is not adjustable. Subwavelength structures provide a way to overcome this restriction on the silicon platform. The refractive index can be reduced by tuning the subwavelength period Λ_{sub} and the subwavelength filling factor f_{sub}. [3–5,7,9,10]. The drawback of this approach is that the decrease in the average effective index of the grating decreases the index contrast between the cladding materials and the grating. As a result, the incident light would easily leak into the cladding, and higher-order diffractions become difficult to suppress [16]. In this Letter, we propose and experimentally verify another possible method to suppress the waveguide dispersion of subwavelength structures. Through combining this method with previous approaches, such as reducing refractive index via decreasing the subwavelength structure pitch and/or increasing the grating period, a wideband grating coupler has been demonstrated with an average refractive index higher than that shown in previous publications [5].

The subwavelength structure is illustrated in the inset of Fig. 1(a). The structure is formed by interleaving silicon and air along the y direction with a period of Λ_{sub} in a 250 nm thick single crystal silicon device layer in a silicon-on-insulator wafer with an oxide thickness of 3 μm and a handle wafer thickness of 650 μm. The width of the air trenches is labeled as W_{air}, and the filling factor of subwavelength structures is defined as $f_{\mathrm{sub}} = W_{\mathrm{air}}/\Lambda_{\mathrm{sub}}$. The wave vector k is along the z direction. The structure was investigated with two-dimensional (2D) plane wave expansion (PWE), [17] and the transverse electric (TE) fundamental modes of the different subwavelength structures with filling factors

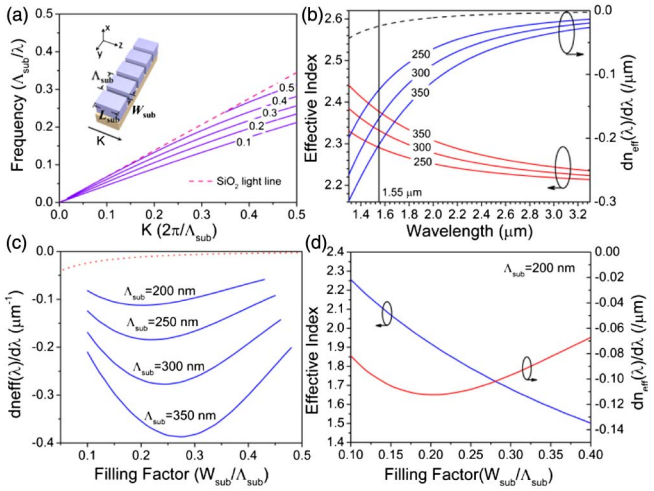

Fig. 1. (a) Fundamental modes of subwavelength structure with filling factor s of 0.1–0.5. (b) Effective index versus wavelength (red), and waveguide dispersion versus wavelength (blue), assuming $f_{sub} = 0.1$. The black dash line is the estimated material dispersion of subwavelength structures for $f_{sub} = 0.1$. (c) Waveguide dispersion versus the filling factor for $\Lambda_{sub} =$ 200, 250, 300, and 350 nm The red dot line is the estimated material dispersion of subwavelength structure at 1.55 μm. (d) Effective index versus filling factor (blue), and waveguide dispersion versus filling factor (red) for $\Lambda_{sub} = 200$ nm.

ranging from 0.1 to 0.5 are plotted in Fig. 1(a) [18]. Only the modes under the SiO_2 light line, representing the practical guided modes, were considered. The effective index of a silicon slab waveguide ($n_{si} = 2.9$) was used in the 2D simulation. As the air filling factor was increased from 0.1 to 0.5, the fundamental modes were shifted to higher frequencies. For modes with a small normalized eigenfrequency, in which Λ_{sub} is much smaller than the wavelength of interest, the modes are weakly confined inside the silicon region. The waveguide dispersion is small in this case because the field distribution is not sensitive to variations in wavelength. As the normalized eigenfrequency increases to a point that Λ_{sub} is comparable to half of the wavelength inside the waveguide, more of the field tends to be confined inside the silicon region. A large portion of field localizes at the silicon and air boundary, indicating that the waveguide dispersion is high. To give an example, the effective index and waveguide dispersion versus wavelength when $f_{sub} = 0.1$ for $\Lambda_{sub} = 250$, 300, and 350 nm are plotted in Fig. 1(b). When Λ_{sub} is a constant, $|dn_{eff}(\lambda)/d\lambda)|$ decreases as the working wavelength increases, and tends to saturate for a wavelength larger than 2 μm. At the wavelength of interest ($\lambda = 1550$ nm), $|dn_{eff}(\lambda)/d\lambda|$ decreases as Λ_{sub} decreases. For instance, when $\Lambda_{sub} = 250$ nm, the waveguide dispersion is around –0.12/μm, which is about half of the value when $\Lambda_{sub} = 350$ nm (~ -0.21/μm). Figure 1(c) further confirms this trend by showing that the waveguide dispersion of subwavelength structures with different Λ_{sub} and f_{sub} at 1550 nm. For f_{sub} between 0.15 and 0.4, the range that designs usually fall in, the waveguide dispersion decreases as the Λ_{sub} decreases. Therefore, a small Λ_{sub} should be chosen to reduce the waveguide dispersion. Unfortunately, to relieve fabrication difficulty, usually a large Λ_{sub} is chosen, which is close to 400 nm [5,19]. These curves also indicate that the waveguide dispersion is smaller at longer wavelengths, so grating couplers working at longer wavelengths could have a much larger bandwidth with the same subwavelength structure. For design convenience, the effective index versus filling factor relation (at $\lambda = 1.55$ μm) when $\Lambda_{sub} = 200$ nm is extracted from Figs. 1(a) and 1(b), and plotted in 1(c). The corresponding waveguide dispersion is also plotted in the same figure, which shows that the waveguide dispersion can be kept less than –0.12/μm when $\Lambda_{sub} = 200$ nm [10].

The benefits of using PWE method is that the results are scalable [18], but the method cannot take material dispersion into consideration, which is also an important factor. The refractive index of bulk silicon can be approximated by the formula [20]

$$n_{si}^2 - 1 = \frac{10.6684293\lambda^2}{\lambda^2 - 0.301516485^2} + \frac{0.003043475\lambda^2}{\lambda^2 - 1.13475115^2} + \frac{1.54133408\lambda^2}{\lambda^2 - 1104.0^2}. \quad (2)$$

Then the material dispersion of bulk silicon can be calculated by $(dn_{si}/d\lambda)$. The material dispersion (TE) of subwavelength structures can be calculated by differentiating the zero-order approximation of effective medium theory (EMT) over wavelength

$$\frac{dn_{sub}^{TE}}{d\lambda} = \left(\frac{f_{sub}n_{si}^2}{n_{air}^2} + 1 - f_{sub}\right)^{-1.5}(1 - f_{sub})\left(\frac{dn_{si}}{d\lambda}\right). \quad (3)$$

The material dispersion of subwavelength structures with different filling factors can be calculated by substituting Eq. (2) into Eq. (3). The dash line in Fig. 1(b) shows the material dispersion of subwavelength structures with $f_{sub} = 0.1$. The dot line in Fig. 1(c) shows the material dispersion of subwavelength structures of different f_{sub} at 1.55 μm. The two curves indicate that the material dispersion of subwavelength structure is small compared to the waveguide dispersion of subwavelength structures. For example, the material dispersion of the subwavelength structure with $f_{sub} = 0.1$ is 0.02 μm^{-1}, while the waveguide dispersion is above 0.1 μm^{-1}. Furthermore, according to Eq. (3), the material dispersion of the subwavelength structure is independent of Λ_{sub}. Thus the discussion still holds that reducing the Λ_{sub} can reduce the waveguide dispersion.

To experimentally demonstrate the theoretical analysis, a set of subwavelength grating couplers with the same grating period Λ_G (0.685 μm) as that in [10], grating filling factor f_G (0.5), high index (silicon, 3.476), and low index (subwavelength structure, 2.45), but with different subwavelength periods Λ_{sub}, were fabricated. In this Letter, $\Lambda_{sub} = 350$, 300, and 250 nm were chosen, with air trench widths of 64, 47, and 34 nm, corresponding to f_{sub} of 18%, 16%, and 14%, respectively, which are calculated with EMT [10]. An increase in bandwidth is expected according to the analysis in the previous section. The grating region is 10 μm wide and 17 μm long to match the near field mode size of an SMF. To characterize the gratings, two identical gratings were connected

by a 2.5 μm wide waveguide, which has negligible propagation loss. The taper could excite higher-order modes, which could make the coupling efficiency less than expectation. The gratings and the waveguide were bridged through 500 μm long adiabatic tapers [10]. The gratings were fabricated on silicon-on-insulator with a 250 nm thick top silicon layer and a 3 μm thick buried oxide layer. To fabricate structures with a minimum feature size of 34 nm, a layer of 27 nm silicon dioxide was deposited with plasma enhanced chemical vapor deposition, which served as a hard mask. The hard mask was patterned with electron beam lithography and reactive ion etching (RIE). The pattern was transferred to the silicon layer through another RIE process, leaving a ~10 nm silicon dioxide hard mask on top. The scanning electron microscope (SEM) images of a fabricated grating are shown in Fig. 2(a). Figures 2(b)–2(d) show the SEM images of subwavelength structures with different Λ_{sub}. The gratings were tested with the setup shown in [10]. The input and output fibers were tilted 10 degrees from normal incidence away from the waveguides. The measured transmission spectra from the grating pairs are shown in Fig. 3(a). The variations in peak wavelength and coupling efficiency have been observed due to the fabrication variations across a single chip and different silicon dioxide residue thicknesses [8]. Nevertheless, the increase in bandwidth is prominent, as summarized in Fig. 3(b), together with the result shown in [10]. The 3 dB bandwidth increases by ~11 nm when Λ_{sub} reduces from 388 to 250. Specifically, $\Lambda_{sub} = 250$ nm gives a 3 dB bandwidth of 63 nm, which is ~20% larger than the unoptimized dispersion case presented in [10]. Theoretically, even larger bandwidth is expected if Λ_{sub} can be shrunk further. The improvement is also limited by the fact that the high index regions of the gratings are still ordinary waveguides with large waveguide dispersion.

The theoretical analysis and the experimental results demonstrated that the waveguide dispersion can be controlled by reducing the period of subwavelength structures. It would be of great interest to combine this method together with other approaches in hope of achieving larger bandwidth. An intuitive way is interleaving dispersion engineered subwavelength structures, as shown in Fig. 4. The grating period Λ_G, effective indices of high and low index regions, and the grating filling factor f_G were scanned through the open source software CAMFR while treating the subwavelength structure as a uniform material based on EMT. A detailed description of the simulation procedure can be found in [10]. The optimized Λ_G is 1.24 μm, and f_G is 0.5. The refractive index

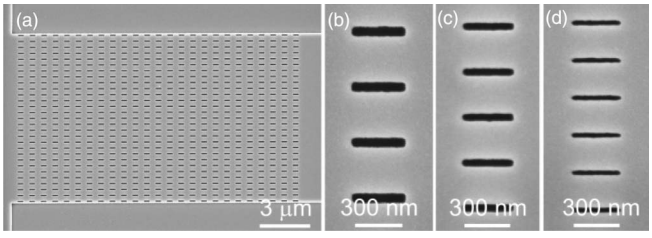

Fig. 2. (a) SEM picture of a subwavelength grating coupler. (b)–(d) SEM pictures of subwavelength structures with $\Lambda_{sub} = 350$, 300, and 250 nm.

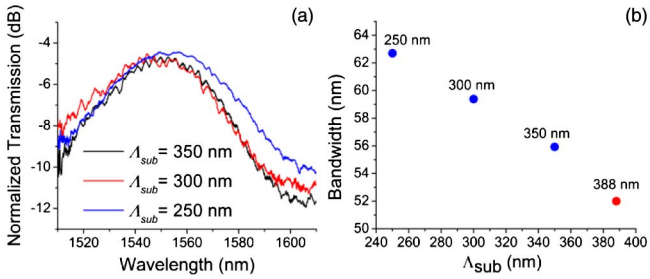

Fig. 3. (a) Transmission spectra of subwavelength structures with different Λ_{sub}, (b) bandwidth versus Λ_{sub}. The red dot is from [10].

of the high index region is 2.55 and that of the low index region is 1.75. The corresponding filling factors for the subwavelength structures are 0.20 (40 nm) and 0.43 (86 nm), respectively, which were calculated by performing a spline fit on the effective index versus filling factor curve in Fig. 1(c). Since both the high and the low index regions are comprised of subwavelength structures, the relative positions of the subwavelength trenches in the x direction have various possibilities. In this paper, two types of morphologies have been fabricated, as shown in Figs. 4(b) and 4(c). One is with aligned air holes between the two sets [Fig. 4(b)], and the other is with air holes of one set shifted by half a subwavelength period Λ_{sub}, with respect to the other set [Fig. 4(c)]. The one with aligned subwavelength trenches are similar as the grating presented in [11], but the structures are with smaller period to reduce the waveguide dispersion. The testing structure and setup are the same as before. Index matching oil is used to reduce reflections and to shift the grating emission angle θ to ~16 degrees. The grating is 13 μm wide and 17 μm long. A larger grating width is used to accommodate the large emission angle and reduce the alignment difficulty caused by the index matching oil. The blue and red solid curves show the transmission spectra of the gratings. The SEM images of the fabricated gratings are shown in the inset of Fig. 5. Both gratings demonstrate almost similar performance, except that the grating with aligned air holes has slightly higher Fabry–Perot fringes. The 1 and 3 dB bandwidths of the two types of grating couplers are ~70 and ~117 nm, respectively. The peak efficiencies are

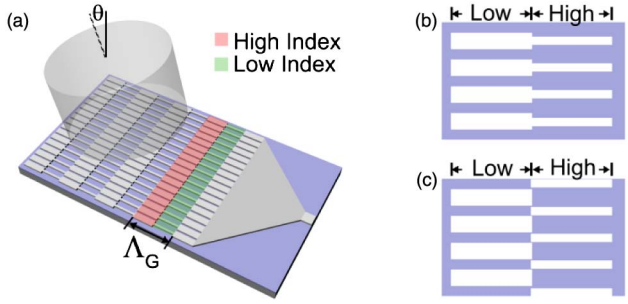

Fig. 4. (a) Schematic of the wideband grating coupler with interleaved subwavelength structures. In this paper, two different types of geometries were investigated. One is with aligned air holes between the two sets, as shown in (b), and the other is with air holes of one set shifted by half a subwavelength period Λ_{sub}, with respect to the other set, as shown in (c).

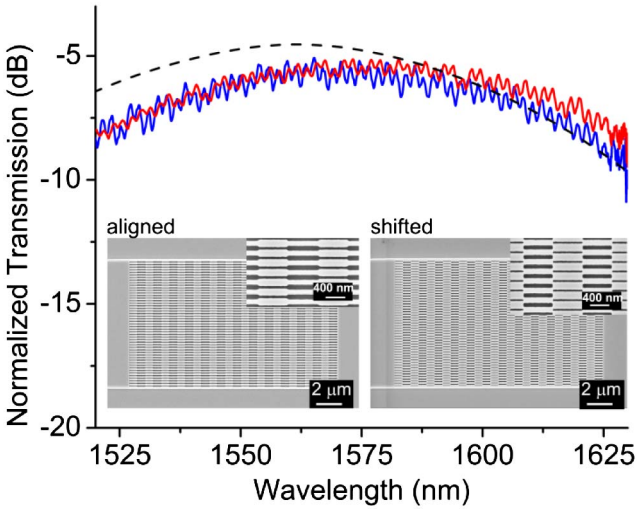

Fig. 5. Transmission spectra for wideband grating coupler with aligned (blue) and shifted subwavelength structures (shifted). Inset: fabricated wideband grating coupler with aligned subwavelength structures (left) and shifted subwavelength structures shifted (right). The dash line is the simulated transmission spectrum.

~5.1 dB at 1570 nm. The dash line is the 2D finite-difference time-domain (FDTD) simulation of the transmission spectrum using EMT without considering the dispersion engineering described in this paper. It shows a 1 dB bandgap of 58 nm, indicating the dispersion engineering described in this paper adds on an extra 12 nm to the bandwidth. The 1 dB bandwidth is more than 2× larger compared to subwavelength gratings demonstrated on similar platforms [10]. Additionally, compared to the single dispersion reduced structure results shown in Fig. 3, there is more than a 50 nm increment in the 3 dB bandwidth. This is the result of combining the factors that affect the bandwidth, including (1) lowering the effective index, (2) using a longer grating period, and (3) shrinking the period of the subwavelength structures. However, these methods and the index matching oil reduce the index contrast. Therefore, the higher-order radiation modes cannot be suppressed unless the grating was apodized, thus, the coupling efficiency is compromised. Further design optimization, including apodization, is required to achieve comparable coupling efficiency to that of higher refractive index contrast couplers.

In conclusion, we investigated the dispersion characteristics of subwavelength structures. We also proposed and experimentally demonstrated suppression of waveguide dispersion by reducing the subwavelength period. Wideband grating couplers based on interleaved dispersion engineered subwavelength structures were designed and fabricated. The gratings demonstrate a coupling efficiency of ~5.1 dB, a 1 dB bandwidth around 70 nm, and a 3 dB bandwidth around 117 nm. The results can be extended to a longer wavelength where the fabrication challenges are smaller.

This research was funded by the Air Force Office of Scientific Research (AFOSR) Multidisciplinary University Research Initiative (MURI) program (Contract No. FA 9550-08-1-0394). and STTR (Contract No. FA9550-11-C-0014) monitored by Dr. Gernot Pomrenke.

References

1. M. Asghari and A. V. Krishnamoorthy, Nat. Photonics **5**, 268 (2011).
2. M. Lipson, J. Lightwave Technol. **23**, 4222 (2005).
3. P. Cheben, P. J. Bock, J. H. Schmid, J. Lapointe, S. Janz, D. X. Xu, A. Densmore, A. Delage, B. Lamontagne, and T. J. Hall, Opt. Lett. **35**, 2526 (2010).
4. P. Cheben, D. X. Xu, S. Janz, and A. Densmore, Opt. Express **14**, 4695 (2006).
5. X. Chen, K. Xu, Z. Z. Cheng, C. K. Y. Fung, and H. K. Tsang, Opt. Lett. **37**, 3483 (2012).
6. Z. Z. Cheng, X. Chen, C. Y. Wong, K. Xu, and H. K. Tsang, Appl. Phys. Lett. **101**, 101104 (2012).
7. R. Halir, P. Cheben, J. H. Schmid, R. Ma, D. Bedard, S. Janz, D. X. Xu, A. Densmore, J. Lapointe, and I. Molina-Fernandez, Opt. Lett. **35**, 3243 (2010).
8. R. Halir, L. Zavargo-Peche, D. X. Xu, P. Cheben, R. Ma, J. H. Schmid, S. Janz, A. Densmore, A. Ortega-Monux, I. Molina-Fernandez, M. Fournier, and J. M. Fedeli, Opt. Quantum Electron. **44**, 521 (2012).
9. H. Subbaraman, X. Xu, J. Covey, and R. T. Chen, Opt. Express **20**, 20659 (2012).
10. X. Xu, H. Subbaraman, J. Covey, D. Kwong, A. Hosseini, and R. T. Chen, Appl. Phys. Lett. **101**, 31109 (2012).
11. Z. Z. Cheng, X. Chen, C. Y. Wong, K. Xu, and H. K. Tsang, Opt. Lett. **37**, 5181 (2012).
12. T. Shoji, T. Tsuchizawa, T. Watanabe, K. Yamada, and H. Morita, Electron. Lett. **38**, 1669 (2002).
13. S. J. McNab, N. Moll, and Y. A. Vlasov, Opt. Express **11**, 2927 (2003).
14. M. Pu, L. Liu, H. Ou, K. Yvind, and J. M. Hvam, Opt. Commun. **283**, 3678 (2010).
15. V. R. Almeida, R. R. Panepucci, and M. Lipson, Opt. Lett. **28**, 1302 (2003).
16. Z. Xiao, T. Y. Liow, J. Zhang, P. Shum, and F. Luan, Opt. Express **21**, 5688 (2013).
17. M. Qiu, Appl. Phys. Lett. **81**, 1163 (2002).
18. J. D. Joannopoulos, S. G. Johnson, J. N. Winn, and R. D. Meade, *Photonic Crystals: Molding the Flow of Light*, 2nd ed. (Princeton University, 2008).
19. X. Xu, H. Subbaraman, J. Covey, D. Kwong, A. Hosseini, and R. T. Chen, Appl. Phys. Lett. **101**, 031109 (2012).
20. M. Bass, C. DeCusatis, J. Enoch, V. Lakshminarayanan, G. Li, C. MacDonald, V. Mahajan, and E. V. Stryland, *Handbook of Optics* (McGraw-Hill, 2009).